Assume a low-speed airplane with thrust independent of airspeed

$$T = \text{const} \tag{11}$$

$$C_D = C_{DO} + C_L^2/(\pi eA) \tag{12}$$

$$C_M = C_{MO} + sC_L \tag{13}$$

Then

$$\delta T = 0 \tag{14}$$

$$\delta L = L(\delta C_L/C_L + 2\delta V/V) = mg(\delta C_L/C_L + 2\delta V/V) \tag{15}$$

$$\delta D = D(\delta C_D/C_D + 2\delta V/V) = \eta^{-1}mg2\delta C_L/(\pi eA) + 2\delta V/V) \tag{16}$$

$$M = M(\delta C_M/C_M + 2\delta V/V) = scmg\delta C_L/C_L - z_T c\eta^{-1}mg2\delta V/V \tag{17}$$

Equation (10) enforces $\delta M = 0$ which in turn implies

$$\delta C_L/C_L = (2/\eta)(z_T/s) \tag{18}$$

This entails

$$\delta L = 2mg[1 + \eta^{-1}(z_T/s)]\delta V/V \tag{19}$$

$$\delta D = 2\eta^{-1}mg[1 + 2(z_T/s)C_L/(\pi eA)]\delta V/V \tag{20}$$

When these are substituted in Eqs. (8) and (9), the equations of motion for δV and $\delta\gamma$ emerge as

$$\delta\dot{\gamma} = (2g/V^2)[1 + \eta^{-1}(z_T/s)]\delta V \tag{21}$$

$$\delta\dot{V} = -2\eta^{-1}(g/V)[1 + 2(z_T/s)C_L/(\pi eA)]\delta V - g\delta\gamma \tag{22}$$

Finally, δV may be solved for from Eq. (21) and substituted in Eq. (22). This results in

$$\delta\ddot{\gamma} + 2\eta^{-1}(g/V)[1 + 2(z_T/s)C_L/(\pi eA)]\delta\dot{\gamma} + 2(g/V)^2[1 + \eta^{-1}(z_T/s)]\delta\gamma = 0 \tag{23}$$

From this last equation the frequency and damping of the phugoid may be read off as

$$\omega = 2^{1/2}(g/V)(1 + \eta^{-1}z_T/s)^{1/2} \tag{24}$$

$$\zeta = (1/2^{1/2}\eta)(1 + \eta^{-1}z_T/s)^{-1/2}[1 + (2C_L/\pi eA)z_T/s] \tag{25}$$

Discussion

In Eqs. (24) and (25), the first factor on the right is the usual expression for the phugoid with $z_T = 0$. The other factors are corrections due to z_T. It is seen that the pertinent parameter is z_T/s. The static margin s is negative for a statically stable airplane. A positive z_T (i.e., thrust line below the c.g.) results in lowering the frequency and damping ratio of the phugoid.

For excessively large negative values of z_T/s, the factors on the right-hand side of Eqs. (24) and (25) may reach zero. When the last factor in Eq. (25) reaches zero, the oscillations become undamped. Further increase of z_T makes the damping negative and leads to divergent oscillations. When the last factor in Eq. (24) becomes small, the natural frequency decreases. At the same time $|\zeta|$ which is proportional to the inverse of this factor increases. Eventually $|\zeta|$ goes through 1 and exponential rather than oscillatory behavior results. If this happens after ζ has become negative, the phugoid motion is changed into exponential divergence. These effects are enhanced by small η and by high C_L.

A General Airplane

For a general airplane the variations in lift, drag, thrust, and aerodynamic moment are subject to various effects, including dependence on Mach number, and explicit expressions are not available. The analysis just presented may still be performed in terms of stability derivatives. When this is done, Eqs. (24) and (25) are replaced by

$$\omega = (-C_{zu}/C_L)^{1/2}(g/V)[1 - (C_{z\alpha}/C_{zu})C_{mu}/C_{m\alpha}]^{1/2} \tag{26}$$

$$\zeta = -\frac{\frac{1}{2}C_{xu}}{(-C_LC_{zu})^{1/2}}\left(1 - \frac{C_{z\alpha}}{C_{zu}}\frac{C_{mu}}{C_{m\alpha}}\right)^{-1/2}\left(1 - \frac{C_{x\alpha} - C_L}{C_{xu}}\frac{C_{mu}}{C_{m\alpha}}\right) \tag{27}$$

It is seen that the parameter that takes the role of z_T/s is

$$C_{mu}/C_{m\alpha}$$

The thrust line displacement z_T manifests itself in C_{mu} which for the simple airplane of the last section becomes $-2C_Dz_T$. The stability derivative C_{mu} is most often neglected.[1] It should be realized that the smallness of C_{mu} is vital to the conventional analysis of the longitudinal modes. If C_{mu} is appreciable, the angle of attack is no longer decoupled from the phugoid motion and the phenomena described above result. Also the airspeed is no longer decoupled from the short period mode. This last point, however, is outside the scope of the present Note.

Reference

[1] Perkins, C. D. and Hage, R. E., *Airplane Performance Stability and Control*, 11th ed., Wiley, New York, 1967, pp. 389–403.

Vortex Flow over Helicopter Rotor Tips

John D. Hoffman* and Henry R. Velkoff†
The Ohio State University, Columbus, Ohio

Introduction

As part of a recent study into the boundary-layer flow on helicopter rotor blade tips at The Ohio State University, flow visualization tests were conducted to reveal local flow direction at many points on various shaped tips. One particularly interesting set of flow traces was obtained with a square tip configuration. This Note presents some of the highlights of that study.

Flow Visualization Technique

The flow over the tips was studied by using a flow visualization technique whereby ammonia vapor was expelled (over a short time duration) from a network of orifices in the tip and carried by the boundary-layer flow over a diazonium salt

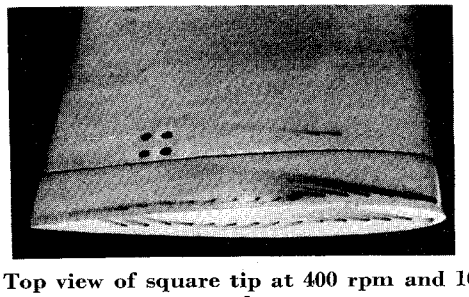

Fig. 1 Top view of square tip at 400 rpm and 10° pitch angle.

Received March 26, 1971. This work was sponsored by the Eustis Directorate, U.S. Army Air Mobility Research and Development Laboratory, Ft. Eustis, Va.

Index Categories: Rotary Wing and VTOL Aerodynamics; Airplane and Component Aerodynamics.

* Graduate Research Assistant, Department of Mechanical Engineering.

† Professor, Department of Mechanical Engineering.

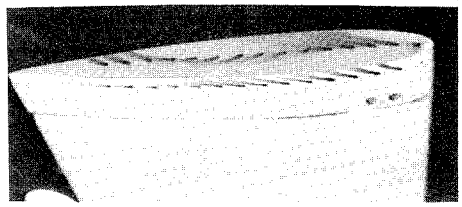

Fig. 2 Bottom view of square tip at 400 rpm and 10° pitch angle.

solution which was sprayed onto the tip. The ammonia vapor reacted with the diazonium salt solution and left dark traces on the surface indicative of the local flow direction. Photographs were taken of the tip following a test. The model rotor had a diameter of approximately 8 ft and had a 9-in. chord. The tests were conducted at 400 rpm resulting in a tip Reynolds number of 8×10^5. Tests at rotor blade pitch angles from 0° to 16° in 2° increments were performed.

Results with Square Tip

Figures 1 and 2 show a typical set of flow traces on the upper, end, and lower surfaces of the square tip at 400 rpm and 10° pitch angle. The traces on the upper surface reveal that the flow direction changes from inward to outward at the seventh hole from the leading edge. Also, the traces on the end of the tip indicate that the flow direction changes from upward to downward at the same distance back from the leading edge. These sudden changes in flow direction on the tip indicate the point of vortex inception. The flow traces on the lower surface indicate outflow over most of the blade except near the trailing edge where the flow moves in a chordwise direction.

Figure 3 depicts schematically the general flow pattern around the square tip. Three regions can be discerned, namely the first ~30% chord, ~30% to ~70% chord, and finally the last ~30% chord. In the first region, the flow rolls up around the tip and spills over onto the upper surface because of the strong pressure gradient which exists between the upper and lower surfaces. In the second region, the magnitude of the flow from the lower surface to the upper surface reaches a higher level and results in the formation of secondary vortices on the end and top surfaces of the tip as shown in Sec. B-B. The local direction of the flow within

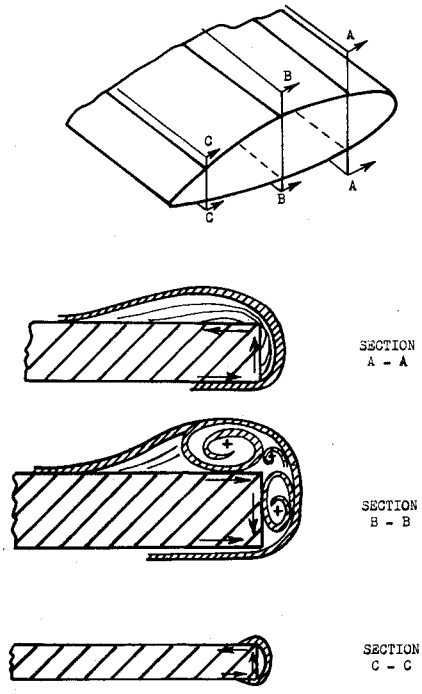

Fig. 3 Sketch of flow patterns around square tip.

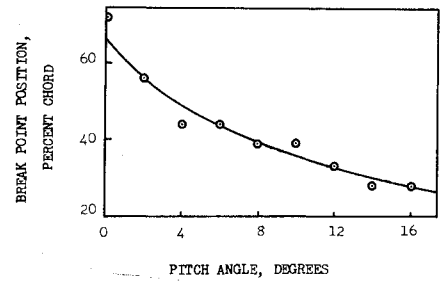

Fig. 4 Point at which traces change direction from inward to outward on upper surface of square tip vs pitch angle.

these vortices accounts for the outward and downward direction of the traces in these regions of the tip. The nature of the flow pattern in the last region is not as clearly defined, but some upward flow is indicated on the end of the tip from Figs. 1 and 2, and is shown in Sec. C-C.

It was found that the point at which the flow direction suddenly changes, i.e., the point of vortex inception, was a strong function of blade pitch angle. From examination of traces, the break point position, i.e., the point at which the traces turned from inward to outward, was determined and plotted as a function of pitch angle in Fig. 4. Figure 4 shows that the point of inception of the tip vortex varies from approximately 30% chord at 16° pitch angle to approximately 70% chord at 0° pitch angle.

The flow patterns that were found to exist on the rotor blade tips may also exist on the tips of regular wings. The ammonia trace technique utilized in these tests may prove useful in any such investigation of fixed wing tips as well as studying a number of surface flows on aircraft such as at inlet regions.

Real Gas Effects in Compressors for Aircraft Gas Turbines

ALLEN E. FUHS*
Naval Postgraduate School, Monterey, Calif.

THE trend to higher and higher pressure ratios in aircraft gas turbines leads to higher exit temperatures from the compressor. The vibrational degrees of freedom of oxygen begin to be thermally excited resulting in a decrease of the ratio of specific heats. The contribution of vibrational degrees of freedom to the heat capacity at constant volume is

$$C_{V,VIB}/R = [(\theta_V/2T)/\sinh(\theta_V/2T)]^2 \qquad (1)$$

Equation (1) is based on the assumption of a harmonic oscillator. For oxygen the characteristic vibrational temperature

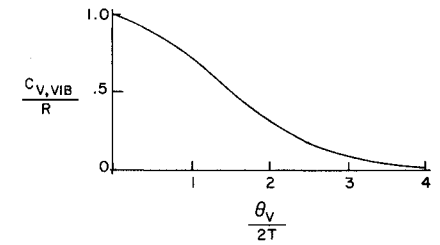

Fig. 1 Vibrational contribution to heat capacity.

Received March 17, 1971. This work was sponsored by the Eustis Directorate, U.S. Army Mobility Research and Development Laboratory, Ft. Eustis, Va.

* Professor, Department of Aeronautics. Associate Fellow AIAA.